crystals

MDPI

Article

Laser-Induced Graphene on a Quartz Crystal Microbalance for Humidity Sensing

Jihun Choi [1], Saeyeon Baek [2], Sangmin Jeon [1] and Changyong Yim [2,3,*]

[1] Department of Chemical Engineering, Pohang University of Science and Technology (POSTECH), Pohang 37674, Korea; jhchoi4@postech.ac.kr (J.C.); jeons@postech.ac.kr (S.J.)
[2] School of Nano & Materials Science and Engineering, Kyungpook National University (KNU), Sangju 37224, Korea; sy.baek@knu.ac.kr
[3] Department of Advanced Science and Technology Convergence, Kyungpook National University (KNU), Sangju 37224, Korea
* Correspondence: cy.yim@knu.ac.kr

Abstract: In this study, a simple method for synthesizing graphene layer directly on a quartz crystal microbalance (QCM) using a laser was developed. This laser-induced graphene (LIG) was used for sensing surface to simultaneously measure changes in the adsorbed mass, film stiffness, and electrical resistance during water adsorption. The developed LIG-QCM is convenient because its fabrication process is free of any tedious masking and vacuuming steps. A thin layer of polyimide (PI) film was spin-coated on one side of a quartz crystal microresonator, and interdigitated electrodes (IDE) were patterned on the PI surface using a laser engraver. The adsorption of water molecules on the sensing surface induced changes in mass, stiffness, and electrical conductivity, which were measured from the changes in resonance frequency, *Q* factor of the quartz crystal, and electrical resistance, respectively. The results indicated that the developed sensor could be a humidity sensing platform using LIG.

Keywords: laser-induced graphene; quartz crystal microbalance; microresonator; gas sensor; multi sensor; humidity sensing

Citation: Choi, J.; Baek, S.; Jeon, S.; Yim, C. Laser-Induced Graphene on a Quartz Crystal Microbalance for Humidity Sensing. *Crystals* **2021**, *11*, 289. https://doi.org/10.3390/cryst11030289

Academic Editor: Ahmad Umar

Received: 23 February 2021
Accepted: 13 March 2021
Published: 15 March 2021

1. Introduction

Polymers have attracted considerable interest as sensing materials owing to the potential applications in gas chromatography, membranes, and gas sensors because of the interactions between gas and polymer. Particularly, gas sensors are widely used to monitor the atmospheric environment or detect hazardous gases [1]. The adsorption of gas molecules onto a polymer surface, a change in mass varies depending on the amount of gas absorbed. The nanostructured or porous polymer films facilitate the diffusion of gas molecules, which shortens the response time of the sensors.

However, polymer gas sensors display several drawbacks including low selectivity [2]. They should detect target gases in mixed gases including moistures, thus the poor selectivity precludes the practical uses of such sensors. These problems can be addressed by combining with additional sensors. The quartz crystal microbalance (QCM) has been evaluated as a gas sensor because it can measure changes in mass and dissipation on its surface accurately at room temperature. Recently, the QCM has been prototyped as a gas sensor by mounting additional electrodes on a single QCM yielding a multichannel system that provides much information about the properties of materials. However, this approach presents a limitation: QCMs and electrical sensors must work separately or the two electrodes can interfere with each other [3–6]. To solve this problem, several studies have attempted to change the structure of the QCM electrodes and integrate orthogonal sensor arrays [7,8]. These integrated systems have multiple sensing mechanisms from the QCM and additional sensor array, and therefore, change in specific manners depending on the target gas type.

To fabricate a QCM gas sensor able to incorporate additional electrodes, the sensing materials should be deposited sequentially on a quartz crystal. Generally, they require a tedious masking and thermal evaporation processes with vacuuming to deposit the electrodes on a quartz crystal [7]. This problem can be addressed by applying a laser process to the polymer-coated QCM to prepare electrodes and sensing materials in one step at room temperature. Laser-induced graphene (LIG) is a carbon nanomaterial that can be easily synthesized using a CO_2 laser to convert polymer films [9–12]. This one-step process is inexpensive, scalable, and compatible with patterning [13]. LIG exhibits high electrical conductivity and high porosity, and because of that, it has been used in several applications like supercapacitors [9,13], adsorbents [14], and sensors [15].

In this study, a novel sensor device that can identify and evaluate various gases by detection on a single integrated sensor was developed. A thin layer of polyimide (PI) film was spin-coated on the front side of the lateral field excitation (LFE)-patterned quartz crystal microresonator and LIG interdigitated electrodes were simply patterned on the film using a CO_2 laser engraver. Changes in resonance frequency, Q factor at the quartz resonator, and electrical resistance at the LIG pattern were measured simultaneously during moisture adsorption. The factors causing each change were studied, and changes in mass, stiffness, and electrical conductivity of the sensing surface during moisture adsorption were measured according to the relative humidity. To the best of our knowledge, this study describes the first integration of LIG patterning and quartz resonator and their application to gas sensors.

2. Materials and Methods

2.1. Materials

QCMs with 5-MHz resonance frequency were purchased from ICM (Oklahoma City, OK, USA). Poly(amic acid) N,N-dimethylacetamide solution was purchased from IPITECH (Daejeon, Korea) and used as a PI precursor. Deionized water (18.3 MΩ·cm) was obtained from a reverse osmosis water system (Human Science, Korea). Acetone was purchased from Samchun chemical (Pyeongtaek, Korea). Gold etchant solution and Ga/In eutectic were purchased from Sigma-Aldrich (St. Louis, MO, USA). Metal shadow masks were obtained from Yesung (Gyeonggi-do, Korea). All chemicals were used without further purification.

2.2. Preparation of QCM

The gold electrodes of the conventional QCM were removed using the gold etchant solution. The metal masks were used to pattern the LFE electrodes on bare QCM. The LFE electrodes were 10 mm in diameter and separated by 1 mm. The bare QCM was cleaned using acetone, then a 10-nm-thick titanium layer and a 100-nm-thick gold layer were deposited sequentially on the QCM by thermal evaporation. The titanium layer was used to achieve adhesion between the quartz surface and gold layer; the gold layer was used as the electrode (Figure 1a).

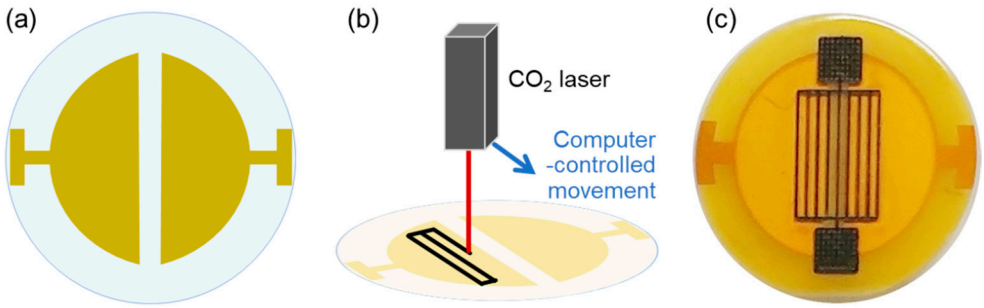

Figure 1. Schematic illustrations of the (**a**) lateral field excitation (LFE) pattern on the backside, (**b**) laser-induced graphene (LIG) process by CO_2 laser. (**c**) an image of polyimide (PI) film and LIG pattern on the front side of a quartz crystal microbalance (QCM).

2.3. Preparation of PI Layer

A 70-mg aliquot of 18 wt% PI precursor solution was loaded on the empty side of the LFE-patterned QCM, spin-coated at 3000 rpm for 30 s, and then dried in ambient condition overnight. Poly(amic acid)-coated QCM was annealed in a 200 °C oven for 2 h.

2.4. Fabrication of Interdigitated Electrodes (IDE)

The LFE QCM coated with PI film was placed on the sample stage of a computer-controlled CO_2 laser engraver (NC GLOBAL, Daejeon, Korea) and the IDE pattern was drawn directly on the PI film by LIG. The pattern included nine sensing lines and two probe pads. The sensing lines were vertically arrayed with 0.5-mm-gaps and connected through horizontal lines. Probe pads were made of a 9 by 9 grid of LIG lines, the laser power was 5.35 W and its speed was 5 mm/s. The patterning processes were performed under ambient conditions (Figure 1b,c).

2.5. Sensing Experiment

As-prepared QCM was mounted in an environmental chamber. Excitation probes were attached to the LFE electrodes of QCM through the bottom of the chamber. Resistance probes were inserted through punched holes of an acryl window that is placed on the top of the chamber using Teflon sealing tape. Then, the probes were connected with the IDE, being supported by drops of Ga/In eutectic. The acryl window was joined with the chamber using an O-ring. The excitation probes were connected to a QCM-Z500 quartz crystal microbalance (KSV Instruments, Helsinki, Finland) to measure changes in resonance frequency and Q factor. The resistance probes were connected to a digital multimeter (Agilent 34410, Agilent Technologies, Santa Clara, CA, USA) to measure changes in electrical resistance (Figure 2a). Nitrogen was used as a carrier gas. Vapors were generated by passing nitrogen gas through deionized water. Two mass flow controllers (MFCs; Brooks Instrument, Hatfield, PA, USA) were used to vary the concentration of vapors: MFC 1 passed dry nitrogen gas, and MFC 2 passed nitrogen gas saturated with the vapor. The total flow rate was 100 sccm. Relative humidity was measured at the outlet of the chamber by using a commercial humidity sensor (Picotech, Cambridgeshire, UK) (Figure 2b).

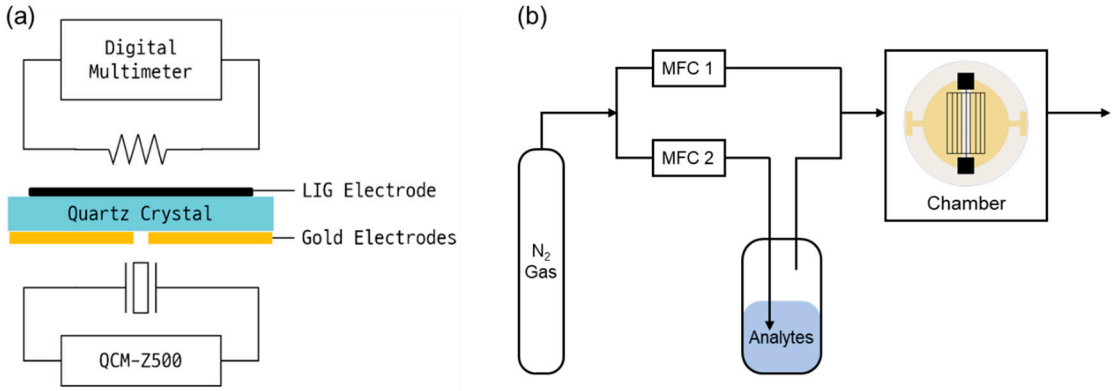

Figure 2. Schematic diagrams of the instrumental setups. (**a**) electrical connections for the QCM and resistance measurement. (**b**) setup for gas sensing.

3. Results and Discussion

The morphology of the PI film was observed using scanning electron microscopy (SEM, Hitachi, Japan). A high-density flat film was formed on the quartz crystal by spin-coating of the poly(amic acid) and thermal annealing process, which shows uniform surface (Figure 3a). The uniformity can increase Q of QCM and induce repeatable signals. The LIG process converted this uniform dense film into porous arc-shaped carbon layers (Figure 3b,c). The porous structures were produced by the rapid liberation of gaseous

products during the LIG process [9,16]. The increase in the strength of laser irradiation along the centerline increased the amount of gas produced, yielding an arc-shaped carbon layer. Consequently, the thickness of the film increased from 7 μm to maximally 34 μm.

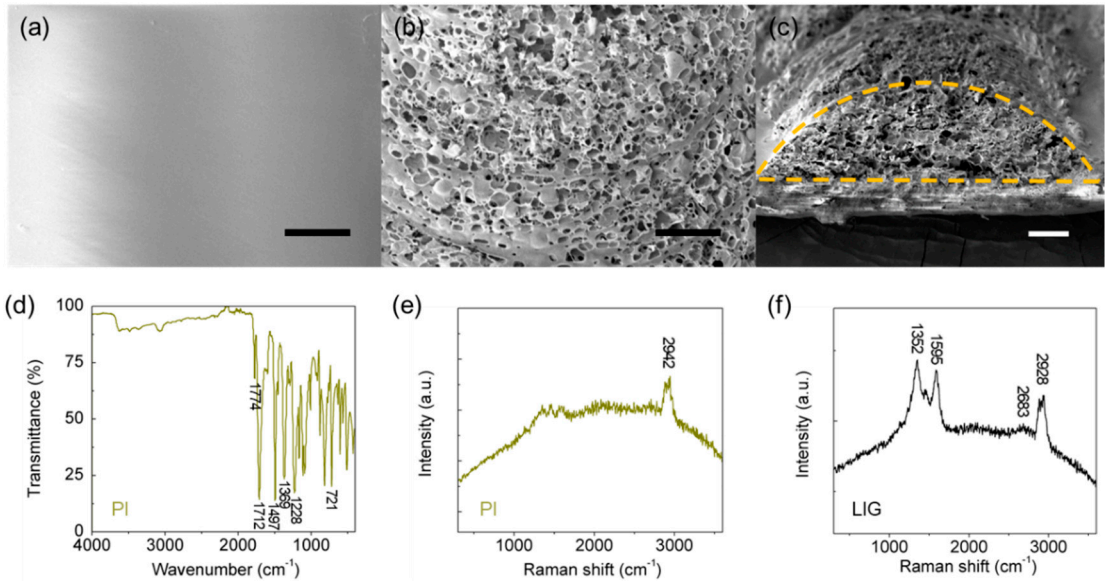

Figure 3. SEM images of (**a**) spin-coated PI film before LIG patterning. SEM images of (**b**) top view and (**c**) cross-sectional view of the on-film fabricated LIG. Scale bars: 20 μm. (**d**) FT-IR spectroscopy result of the PI film. Raman spectroscopy results of (**e**) PI film and (**f**) LIG.

Fabricated LIG was highly porous in both surface and cross-sectional images. The high porosity increased the surface area and provided benefits for gas sensor applications because the amount of gas adsorption can be increased, and the response time can be reduced.

The PI film was also characterized using Fourier-transform infrared spectroscopy (FT-IR) (Figure 3d). The peaks at 1774, 1712, and 1369 cm^{-1} are the characteristic adsorption peaks of PI and were assigned to the C=O asymmetric stretching, C=O symmetrical stretching, and C–N stretching in the imide ring, respectively. The FT-IR data (Figure 3d) contained all characteristic peaks of PI, but these peaks also can be attributed to poly(amic acid); to confirm the conversion to PI after thermal annealing, additional analysis is needed. The PI film and LIG were compared using Raman spectroscopy (Figure 3e,f). After the LIG process, three new peaks appeared in the spectrum: The D peak (1352 cm^{-1}), G peak (1595 cm^{-1}), and 2D peak (2683 cm^{-1}), confirming that graphitic carbon was fabricated [17]. Low graphitic characteristic indicated by the large D peak was the limitation, which can be increased by optimizing the thermal annealing conditions or by changing the atmospheric conditions during the LIG process [18–21].

The changes in resonance frequency, f, electrical resistance, R, and Q factor, Q, were measured simultaneously during moisture sensing (Figure 4a–c). Five cycles were performed with different relative humidities. Each cycle was composed of 10 min of exposure and 20 min of purging. Changes in Q were smoothed by averaging 100 adjacent points. The magnitude of each change at the maximum relative humidity point of each cycle was plotted against the relative humidity (Figure 4d). The values measured after the purging step of each cycle were denominated as f_0, R_0, and Q_0 to analyze the change separately for each cycle and correct the baseline shifts. As the relative humidity increased, f decreased linearly, and R increased linearly; the Q also decreased, concomitant with a gradual increase in the magnitude of the slope.

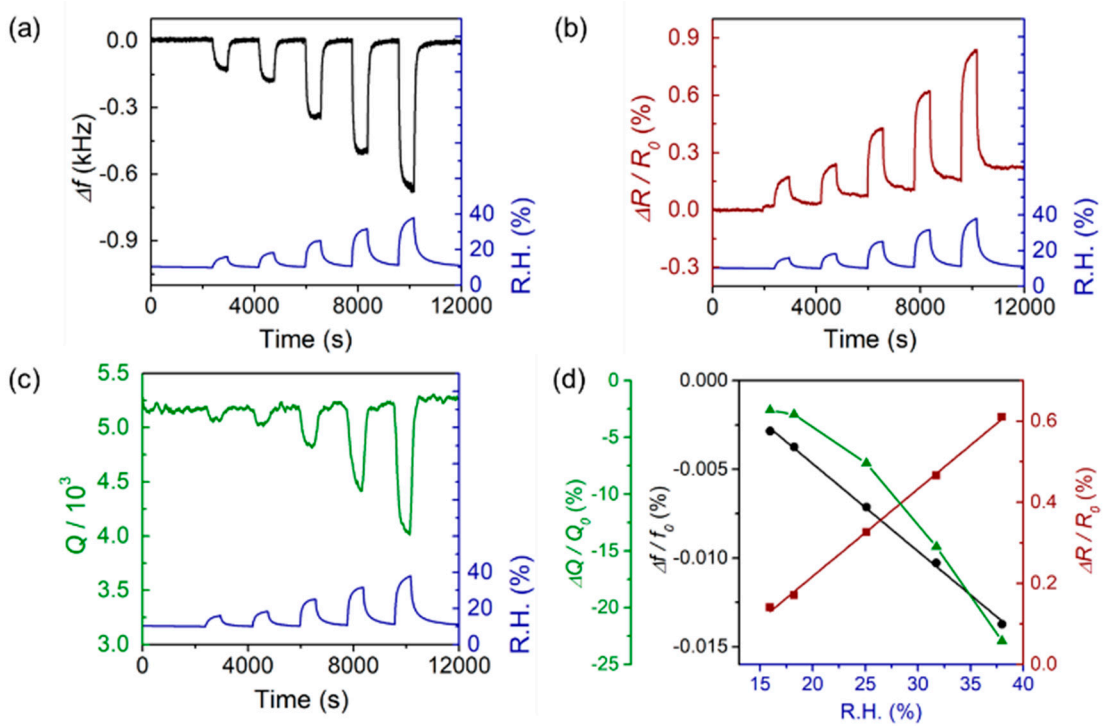

Figure 4. Simultaneously measured (**a**) resonance frequency changes (black), (**b**) electrical resistance changes (red), and (**c**) smoothed *Q* factor changes (green) by varying the relative humidity, which were measured by a commercial humidity sensor (blue). (**d**) the maximum relative measurement of each change for each cycle is plotted by the relative humidity. f_0 = initial resonance frequency during trial; R_0: Original electrical resistance = 1.58 kΩ at t = 0; and Q_0 = initial *Q* factor during trial.

The changes in *f*, *R*, and *Q*, which were measured simultaneously during moisture sensing (Figure 4a–c), were induced by the gas adsorption but the detailed mechanisms differ as follows.

The decrease in *f* represents the increase of the mass on the QCM, as a result of the absorption of water vapor into the PI film and LIG. The Sauerbrey equation shows that Δf is proportional to the mass change [22]. This equation can be applied for a uniform, dense, and thin film on QCM with conventional electrodes. The equation is not suitable to be applied directly on the proposed QCM but Δf is still relative to the number of adsorbed molecules on the QCM surfaces [23,24]. Additionally, the experimental results showed proportional change (Figure 4d).

The increase in the *R*-value of the LIG pattern occurred as a result of the swelling effect. When water vapor is adsorbed into the LIG, the interlayers swell, and consequently, the interlayer distance increases. Then, the degree of connectivity decreases, leading to the increase in *R* [25]. In addition, the high porosity of LIG promotes the absorption of water vapor due to its high surface area so that the more water molecules could be absorbed and easily pass through the pore. In results, the high porosity of LIG can increase the sensitivity and reduce the response time of target molecules compared to non-porous sensing materials such as polymer films.

The *Q* factor is the reciprocal of the dissipation factor and describes the resonator's degree of underdamping. The *Q* factor decreased during the exposure to water vapor and returned to the baseline level during purging (Figure S1). This effect can be explained by the viscoelastic properties of the film. The PI film is hydrophobic but its small pores or defects on the surface provide adsorption sites for water molecules [26,27]. Moisture-adsorbed film changes from rigid to elastic; thus, the *Q* factor decreases [28].

4. Conclusions

A novel quartz crystal resonator able to simultaneously measure changes in mass, film stiffness, and electrical conductivity was developed. Changes in mass and film stiffness were measured by the changes in resonance frequency and Q factor from QCM, respectively. Electrical resistance was measured from a LIG pattern, which was directly patterned on the quartz resonator. Simultaneous measurements were performed under different relative humidity conditions. As the relative humidity increased, f decreased linearly, and R increased linearly; the Q also decreased, concomitant with a gradual increase in the slope magnitude. With the facile fabrication method using LIG process, the developed multichannel sensor can be used as a sensing device, overcoming the low selectivity limitation of the existing gas sensors.

Supplementary Materials: The following are available online at https://www.mdpi.com/2073-4352/11/3/289/s1, Figure S1: Reproducibility of the resonance frequency changes during 10 cycles of humidity sensing.

Author Contributions: Conceptualization, J.C. and C.Y.; methodology, C.Y.; writing—original draft preparation, J.C.; writing—review and editing, S.B. and S.J.; visualization, J.C.; supervision, C.Y.; project administration, S.J. and C.Y.; funding acquisition, C.Y. All authors have read and agreed to the published version of the manuscript.

Funding: This work was supported by the National Research Foundation of Korea (NRF) grant funded by the Korea government (MSIT) (NRF-2020R1G1A1099886).

Institutional Review Board Statement: Not applicable.

Informed Consent Statement: Not applicable.

Data Availability Statement: Not applicable.

Acknowledgments: This work was supported by the National Research Foundation of Korea (NRF) grant funded by the Korea government (MSIT) (NRF-2020R1G1A1099886).

Conflicts of Interest: The authors declare no conflict of interest.

References

1. Yunusa, Z.; Hamidon, M.N.; Kaiser, A.; Awang, Z. Gas Sensors: A Review. *Sens. Transducers* **2014**, *168*, 61–75.
2. Potyrailo, R.A. Multivariable Sensors for Ubiquitous Monitoring of Gases in the Era of Internet of Things and Industrial Internet. *Chem. Rev.* **2016**, *116*, 11877–11923. [CrossRef]
3. Cui, L.; Swann, M.J.; Glidle, A.; Barker, J.R.; Cooper, J.M. Odour Mapping Using Microresistor and Piezo-Electric Sensor Pairs. *Sens. Actuators B Chem.* **2000**, *66*, 94–97. [CrossRef]
4. Hwang, B.J.; Yang, J.Y.; Lin, C.W. Recognition of Alcohol Vapor Molecules by Simultaneous Measurements of Resistance Changes on Polypyrrole-Based Composite Thin Films and Mass Changes on a Piezoelectric Crystal. *Sens. Actuators B Chem.* **2001**, *75*, 67–75. [CrossRef]
5. Goda, T.; Maeda, Y.; Miyahara, Y. Simultaneous Monitoring of Protein Adsorption Kinetics Using a Quartz Crystal Microbalance and Field-Effect Transistor Integrated Device. *Anal. Chem.* **2012**, *84*, 7308–7314. [CrossRef]
6. Wark, M.; Winters, S.; York, C.; Pinkham, W.; Bernhardt, G.; Vetelino, J.F. A Lateral Field Excited Sensor Array on a Single Piezoelectric Substrate. *IEEE Ultrason. Symp.* **2006**, 876–879. [CrossRef]
7. Yim, C.; Yun, M.; Jung, N.; Jeon, S. Quartz Resonator for Simultaneously Measuring Changes in the Mass and Electrical Resistance of a Polyaniline Film. *Anal. Chem.* **2012**, *84*, 8179–8183. [CrossRef] [PubMed]
8. Yu, L.; Huang, Y.; Jin, X.; Mason, A.J.; Zeng, X. Ionic Liquid Thin Layer EQCM Explosives Sensor. *Sens. Actuators B Chem.* **2009**, *140*, 363–370. [CrossRef]
9. Lin, J.; Peng, Z.; Liu, Y.; Ruiz-Zepeda, F.; Ye, R.; Samuel, E.L.G.; Yacaman, M.J.; Yakobson, B.I.; Tour, J.M. Laser-Induced Porous Graphene Films from Commercial Polymers. *Nat. Commun.* **2014**, *5*, 5714. [CrossRef]
10. Lee, S.; Jeon, S. Laser-Induced Graphitization of Cellulose Nanofiber Substrates under Ambient Conditions. *ACS Sustain. Chem. Eng.* **2018**, *7*, 2270–2275. [CrossRef]
11. Lee, S.; Jang, H.; Lee, H.; Yoon, D.; Jeon, S. Direct Fabrication of a Moisture-Driven Power Generator by Laser-Induced Graphitization with a Gradual Defocusing Method. *ACS Appl. Mater. Interfaces* **2019**, *11*, 26970–26975. [CrossRef]
12. Lee, S.; Eun, J.; Jeon, S. Facile Fabrication of a Highly Efficient Moisture-Driven Power Generator Using Laser-Induced Graphitization under Ambient Conditions. *Nano Energy* **2020**, *68*, 104364. [CrossRef]

13. Chyan, Y.; Ye, R.; Li, Y.; Singh, S.P.; Arnusch, C.J.; Tour, J.M. Laser-Induced Graphene by Multiple Lasing: Toward Electronics on Cloth, Paper, and Food. *ACS Nano* **2018**, *12*, 2176–2183. [CrossRef]
14. Rathinam, K.; Singh, S.P.; Li, Y.; Kasher, R.; Tour, J.M.; Arnusch, C.J. Polyimide Derived Laser-Induced Graphene as Adsorbent for Cationic and Anionic Dyes. *Carbon* **2017**, *124*, 515–524. [CrossRef]
15. Garland, N.T.; McLamore, E.S.; Cavallaro, N.D.; Mendivelso-Perez, D.; Smith, E.A.; Jing, D.; Claussen, J.C. Flexible Laser-Induced Graphene for Nitrogen Sensing in Soil. *ACS Appl. Mater. Interfaces* **2018**, *10*, 39124–39133. [CrossRef] [PubMed]
16. Dreyfus, R.W. CN Temperatures above Laser Ablated Polyimide. *Appl. Phys.* **1992**, *55*, 335–339. [CrossRef]
17. Ferrari, A.C.; Meyer, J.C.; Scardaci, V.; Casiraghi, C.; Lazzeri, M.; Mauri, F.; Piscanec, S.; Jiang, D.; Novoselov, K.S.; Roth, S.; et al. Raman Spectrum of Graphene and Graphene Layers. *Phys. Rev. Lett.* **2006**, *97*, 187401. [CrossRef]
18. Inagaki, M.; Harada, S.; Sato, T.; Nakajima, T.; Horino, Y.; Morita, K. Carbonization of Polyimide Film "Kapton". *Carbon* **1989**, *27*, 253–257. [CrossRef]
19. Li, Y.; Luong, D.X.; Zhang, J.; Tarkunde, Y.R.; Kittrell, C.; Sargunaraj, F.; Ji, Y.; Arnusch, C.J.; Tour, J.M. Laser-Induced Graphene in Controlled Atmospheres: From Superhydrophilic to Superhydrophobic Surfaces. *Adv. Mater.* **2017**, *29*, 1700496. [CrossRef]
20. Jou, J.-H.; Huang, P.-T. Effect of Thermal Curing on the Structures and Properties of Aromatic Polyimide Films. *Macromolecules* **1991**, *24*, 3796–3803. [CrossRef]
21. Jang, H.; Choi, J.; Lee, H.; Jeon, S. Corrugated Wood Fabricated Using Laser-Induced Graphitization for Salt-Resistant Solar Steam Generation. *ACS Appl. Mater. Interfaces* **2020**, *12*, 30320–30327. [CrossRef] [PubMed]
22. Sauerbrey, G. Verwendung von Schwingquarzen Zur Wägung Dünner Schichten Und Zur Mikrowägung. *Z. Für Phys.* **1959**, *155*, 206–222. [CrossRef]
23. Hu, Y.; French, L.A.; Radecsky, K.; Da Cunha, M.P.; Millard, P.; Vetelino, J.F. A Lateral Field Excited Liquid Acoustic Wave Sensor. *IEEE Trans. Ultrason. Ferroelectr. Freq. Control* **2004**, *51*, 1373–1380. [CrossRef]
24. Meissner, M.; French, L.A.; Pinkham, W.; York, C.; Bernhardt, G.; Cunha, M.P.D.; Vetelino, J.F. Electrode Optimization for a Lateral Field Excited Acoustic Wave Sensor. *IEEE Ultrason. Symp. 2004* **2004**, *1*, 314–318. [CrossRef]
25. Barroso-Bujans, F.; Cerveny, S.; Alegría, A.; Colmenero, J. Sorption and Desorption Behavior of Water and Organic Solvents from Graphite Oxide. *Carbon* **2010**, *48*, 3277–3286. [CrossRef]
26. Kim, J.-H.; Lee, K.-H.; Kim, S.Y. Pervaporation Separation of Water from Ethanol through Polyimide Composite Membranes. *J. Membr. Sci* **2000**, *169*, 81–93. [CrossRef]
27. Subramanian, R.; Potriger, M.T.; Morris, J.H.; Curilla, J.P. Effect of Moisture on The Physical Properties of Polyimide Films. *MRS Online Proc. Libr.* **1991**, *227*, 147. [CrossRef]
28. Björklund, S.; Kocherbitov, V. Humidity Scanning Quartz Crystal Microbalance with Dissipation Monitoring Setup for Determination of Sorption-Desorption Isotherms and Rheological Changes. *Rev. Sci. Instrum.* **2015**, *86*, 055105. [CrossRef]